Experimental

Monodisperse silica colloids with diameters ranging from 200–500 nm are synthesized following the Stober–Fink–Bohn method [47]. The as-synthesized silica sols are purified and redispersed in 200 proof ethanol by at least six centrifugation/redispersion cycles. The methods described in our previous paper [36] are used to fabricate three-dimensionally ordered planar colloidal crystals with thickness ranging from one monolayer to 50 monolayers. In short, a glass slide is immersed vertically into ~15 mL purified silica sol (1 % particle volume fraction) contained in a glass scintillation vial. After ethanol slowly evaporates, an iridescent film is formed on top of the glass slide. A large area (1 cm × 3 cm) sample can be made over 3–5 days. After each single coating is deposited, the film is taken out of the silica sol and air-dried for 10 min and then dipped again into another purified silica sol with differing particle size. This coating–drying–coating cycle can be repeated many times and each time the particle size can be arbitrary selected. The thickness of each crystalline sub-unit can be easily tuned by changing the concentration of the silica sol [36]. In this way, a layered structure with an arbitrary pattern of sphere sizes can be assembled. Macroporous polystyrene films are made by templating the colloidal crystal as described before [18].

SEM is carried out on a Philips XL30 ESEM. A CrC-100 sputtering system has been used to coat a thin layer of gold on the samples before SEM analysis. To reveal an edge appropriate for cross-sectional SEM analysis, the samples are scraped using a sharp razor blade and tilted 30–40°. Transmission spectra are obtained by using an Ocean Optics ST2000 fiber optic UV–near-IR spectrometer. An Oriel model 6000 UV lamp with 68806 basic power supply is used to polymerize styrene.

Received: October 5, 2000

[1] P. Pieranski, *Contemp. Phys.* **1983**, *24*, 25.
[2] A. P. Gast, W. B. Russel, *Phys. Today* **1998**, *51*, 24.
[3] Y. Xia, B. Gates, Y. Yin, Y. Lu, *Adv. Mater.* **2000**, *12*, 693.
[4] W. L. Vos, R. Sprik, A. van Blaaderen, A. Imhof, A. Lagendijk, G. H. Wegdam, *Phys. Rev. B* **1996**, *53*, 16 231.
[5] I. I. Tahran, G. W. Watson, *Phys. Rev. Lett.* **1996**, *76*, 315.
[6] J. D. Joannopoulos, R. D. Meade, J. N. Winn, *Photonic Crystals*: *Molding the Flow of Light*, Princeton University Press, Princeton **1995**.
[7] P. L. Flaugh, S. E. O'Donnell, S. A. Asher, *Appl. Spectrosc.* **1984**, *38*, 847.
[8] E. A. Kamenetzky, L. G. Mangliocco, H. P. Panzer, *Science* **1994**, *263*, 207.
[9] G. Pan, R. Kesavamoorthy, S. A. Asher, *Phys. Rev. Lett.* **1997**, *78*, 3860.
[10] S. Sun, B. Murray, D. Weller, L. Folks, A. Moser, *Science* **2000**, *287*, 1989.
[11] J. H. Holtz, S. A. Asher, *Nature* **1997**, *389*, 829.
[12] O. D. Velev, E. W. Kaler, *Langmuir* **1999**, *15*, 3693.
[13] O. D. Velev, T. A. Jede, R. F. Lobo, A. M. Lenhoff, *Nature* **1997**, *389*, 447.
[14] B. T. Holland, C. F. Blanford, A. Stein, *Science* **1998**, *281*, 538.
[15] G. Subramanian, V. N. Manoharan, J. D. Thorne, *Adv. Mater.* **1999**, *11*, 1261.
[16] S. H. Park, Y. Xia, *Adv. Mater.* **1998**, *10*, 1045.
[17] S. A. Johnson, P. J. Ollivier, T. E. Mallouk, *Science* **1999**, *283*, 963.
[18] P. Jiang, K. S. Hwang, D. M. Mittlman, J. F. Bertone, V. L. Colvin, *J. Am. Chem. Soc.* **1999**, *121*, 11 630.
[19] Y. A. Vlasov, N. Yao, D. J. Norris, *Adv. Mater.* **1999**, *11*, 165.
[20] P. V. Braun, P. Wiltzius, *Nature* **1999**, *402*, 603.
[21] P. Jiang, J. Cizeron, J. F. Bertone, V. L. Colvin, *J. Am. Chem. Soc.* **1999**, *121*, 7957.
[22] O. D. Velev, P. M. Tessier, A. M. Lenhoff, E. W. Kaler, *Nature* **1999**, *401*, 548.
[23] B. J. Ackerson, K. Schatzel, *Phys. Rev. E* **1995**, *52*, 6448.
[24] P. N. Pusey, W. van Megen, *Nature* **1986**, *320*, 340.
[25] J. L. Harland, S. M. Henderson, S. M. Underwood, W. van Megen, *Phys. Rev. Lett.* **1995**, *75*, 3572.
[26] C. Murray, *MRS Bull.* **1998**, *23*, 33.
[27] N. A. Clark, A. J. Hurd, B. J. Ackerson, *Nature* **1979**, *281*, 57.
[28] H. B. Sunkara, J. M. Jethmalani, W. T. Ford, *Chem. Mater.* **1994**, *6*, 362.
[29] M. Weissman, H. B. Sunkara, A. S. Tse, S. A. Asher, *Science* **1996**, *274*, 959.
[30] Z. Cheng, W. B. Russel, P. M. Chalkin, *Nature* **1999**, *401*, 893.
[31] H. Miguez, F. Meseguer, C. Lopez, A. Blanco, J. S. Moya, J. Requena, A. Mifsud, V. Fornes, *Adv. Mater.* **1997**, *10*, 480.
[32] M. Trau, D. A. Saville, I. A. Aksay, *Science* **1996**, *272*, 706.
[33] R. C. Hayward, D. A. Saville, I. A. Aksay, *Nature* **2000**, *404*, 56.
[34] A. van Blaaderen, R. Rue, P. Wiltzius, *Nature* **1997**, *385*, 321.
[35] S. H. Park, D. Qin, Y. Xia, *Adv. Mater.* **1998**, *10*, 1028.
[36] P. Jiang, J. F. Bertone, K. S. Hwang, V. L. Colvin, *Chem. Mater.* **1999**, *11*, 2132.
[37] A. S. Dimitrov, C. D. Dushkin, H. Yoshimura, K. Nagayama, *Langmuir* **1994**, *10*, 432.
[38] N. Hunt, R. Jardine, P. Bartlett, *Phys. Rev. E* **2000**, *62*, 900.
[39] C. J. Kiely, M. Brust, D. Bethell, D. J. Schiffrin, *Nature* **1998**, *396*, 444.
[40] J. V. Sanders, *Philos. Mag. A* **1980**, *42*, 721.
[41] L. V. Woodcock, *Nature* **1997**, *385*, 141.
[42] A. S. Dimitrov, K. Nagayama, *Langmuir* **1996**, *12*, 1303.
[43] J. F. Bertone, P. Jiang, K. S. Hwang, D. M. Mittleman, V. L. Colvin, *Phys. Rev. Lett.* **1999**, *83*, 300.
[44] L. Liu, P. Li, S. A. Asher, *J. Am. Chem. Soc.* **1997**, *119*, 2729.
[45] W. H. Southwell, *Appl. Opt.* **1997**, *36*, 314.
[46] R. R. Bhave, *Inorganic Membranes*: *Synthesis*, *Characteristics and Applications*, Van Nostrand Reinhold, New York **1991**.
[47] W. Stober, A. Fink, E. Bohn, *J. Colloid Interface Sci.* **1968**, *26*, 62.

Synthesis and Photonic Bandgap Characterization of Polymer Inverse Opals**

By *Hernán Míguez*, *Francisco Meseguer*, *Cefe López*,* *Fernando López-Tejeira*, and *José Sánchez-Dehesa*

Systems with spatial periodic modulation of the dielectric constant have attracted much attention from both theorists and experimentalists during the last decade.[1] These structures, known as photonic bandgap materials, would present interesting technological applications in photonics and electronics.[2] Such applications rely on the fabrication of materials with photonic crystal properties in the visible and near infrared. Colloidal systems in general, and opals in particular, have been shown to present photonic crystal properties[3,4] and other advantages in that direction. These systems can be easily fabricated and their work region tuned through the sphere diameter, covering an ample range around the visible and near infrared.[5] However, opals are most appreciated not for their own photonic properties but for their use as hosts to other materials and, especially, as matrices for the molding of inverse opals. Silica opals particularly are very useful in applications where the synthesis of the guest materials require extreme conditions, since silica is thermally stable at relatively elevated temperatures and chemically inert in the presence of most solvents (particularly organic ones).

From a practical point of view the polymer infiltration in opals, whether silica or otherwise, is relatively easy and efficient. Host matrices are also easily removed by means of either a chemical attack or an optically induced degradation;

[*] Dr. C. López, H. Míguez, Dr. F. Meseguer
Instituto de Ciencia de Materiales de Madrid (CSIC)
Cantoblanco, E-28049 Madrid (Spain)
E-mail: cefe@icmm.csic.es
and
Centro Tecnológico de Ondas, Unidad Asociada CSIC-UPV
Edificio Nuevos Institutos II, Universidad Politécnica de Valencia
Av. Naranjos s/n, E-46022 Valencia (Spain)
Dr. F. López-Tejeira, Dr. J. Sánchez-Dehesa
Dep. Física Teórica de la Materia Condensada
Universidad Autónoma de Madrid
Cantoblanco, E-28049 Madrid (Spain)

[**] This work was partially financed by the Spanish CICyT project No. MAT97-0698-C04, European Commission project IST-1999-19009 PHOBOS project, and the Fundación Ramón Areces. We also acknowledge MIT for photonic band structure calculations.

  0935-9648/01/0603-0393 $ 17.50+.50/0

ADVANCED MATERIALS

both procedures being highly selective. In this fashion, an exact replica of the starting material can be obtained.[6,7]

Even though the dielectric contrast in empty inverse opals is not very high ($\varepsilon_{polymer}/\varepsilon_{air}$ = 2.5 or thereabouts), it is higher than that of bare silica opals ($\varepsilon_{silica}/\varepsilon_{air}$ = 2.1). Furthermore, due to the topology being inverse, the filling ratio for the scattering material is low (f = 0.26), which is required to enhance the photonic bandgap properties. Other properties that are usually inherent to polymers, e.g., elasticity, add to the wealth of possible applications of these systems. A precise and controlled variation of the optical signatures of these inverse opals can be achieved by the application of strain to the structure as was demonstrated on latex direct opals.[8] Strong modifications of dye emission have been observed in these sorts of systems when dyes are embedded in the photonic structure.[9]

From a fundamental point of view these systems are interesting since they permit, as will be shown here, the analysis and direct comparison of the effects of topology and index contrast in photonic crystals for the visible and near infrared. Actually, they have already been used to analyze the dependence of the diffraction properties on the crystal thickness.[10] Inverse opals made of polymeric materials could also have a range of applications, not only in photonics. Due to their particular porous structure, they could be used as membranes or as a lattice of spherical micro-reactors in which new materials can be synthesized.

The procedure used to obtain the opals with sphere diameters lower than 550 nm has been extensively described previously.[11] Opals of larger spheres have been obtained using a re-growth method based on the Stöber–Fink–Bohn technique, employing smaller spheres as seeds.[12] In this study we have used opals sintered at 950 °C for 3 h as the starting material (see experimental section). These conditions guarantee that the filling fraction be 0.74 for the silica with a very slight connection between the spheres.[13] This is very important in later stages when the original matrix is removed. It ensures connectivity throughout the structure so that the etchant can reach everywhere and totally remove the silica.

Figure 1 shows scanning electron microscopy (SEM) images of cleft edges of a sample after polishing. The composite regular structure can be seen where some of the silica spheres were detached on cleaving. The inset shows a detail of the surface after polishing. Where the sphere is missing, the windows connecting neighboring voids can be observed. Some spheres are sectioned on polishing revealing the internal structure, which tells more about the processes of growth. The number of shells indicates the number of re-growth processes.

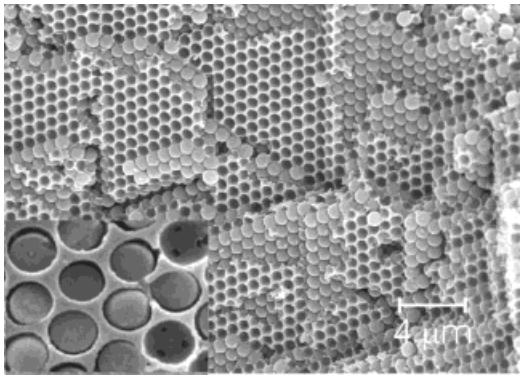

Fig. 1. Polymer infiltrated opal viewed under the SEM. Images of internal {111} type facets with a higher magnification inset of the same kind of face after polishing.

After the polishing stage, the silica is removed from the composite material by means of etching with a 1 wt.-% HF aqueous solution. It was found that 12 h in this solution completely dissolves the silica leaving a neat inverse polymer opal. The polymer is not affected by the silica etching. The necks connecting the silica spheres (resulting from the sintering process) act as channels through which the etchant flows. The good connectivity provided by the sintering allows it to reach the whole structure and fully etch away the silica skeleton. Figure 2 shows an example of the resultant structure after the etching has been performed. The internal {111} type planes are identified by the symmetry, and the quality of the replica

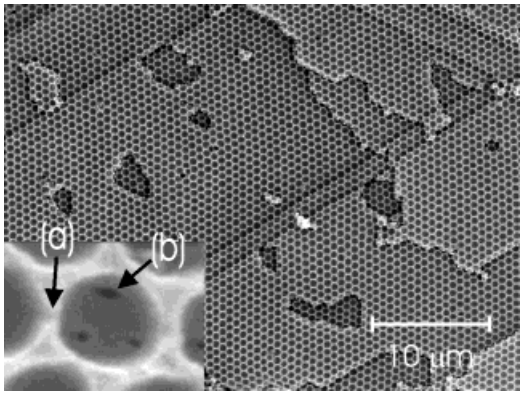

Fig. 2. SEM image of a polymer inverse opal, revealing the perfection of the replication process. The inset shows a detail of one cavity a) where the channels communicating with the spheres in the same layer can be seen, and b) where the three channels communicating with the underlying layer can be seen.

can be appreciated at the cleaved edges. The inset displays the structure of these channels, for the (111) facet there are three that connect to the layer underneath, plus six connecting the surrounding spheres. Of course, the latter six can only be seen in sections through the equatorial plane of the spheres. It is worth mentioning here that all the silica disappears in the etching process. The perfection of this structure is enticing as far as its use as a template for the growth of fine monodisperse spherical particles is concerned. Some materials that otherwise would not grow in this shape due to their crystallinity, can nevertheless be grown in this structure.[14]

Important optical changes due to the infiltration and subsequent inversion can be appreciated even by naked eye. In Figure 3 near normal incidence reflection and transmission images are displayed. The major feature to be observed is the blue shift of the reflected color that will be explained next.

For the optical characterization of the different stages of inverse opal synthesis we have employed both reflectance and transmission spectroscopy. The samples are always oriented with its (111) direction on the optical axis so that the reflec-

  0935-9648/01/0603-0394 $ 17.50+.50/0

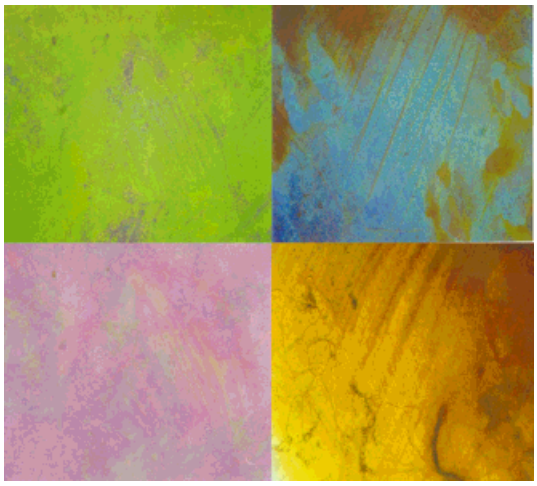

Fig. 3. Reflection (upper) and transmission (lower) images obtained with an optical microscope of 500 × 200 μm^2 regions of an opal made of 230 nm spheres: prior (left), and after (right) infiltration and inversion.

tion observed corresponds to light ***k***-vectors crossing the Brillouin zone boundaries in the vicinity of the *L* point. An example can be seen in Figure 4 where both transmission and angle integrated reflectance are plotted for three opals of 390 nm spheres. The doted line corresponds to the bare opal (74 % silica, 26 % air); the dashed line to the fully infiltrated opal

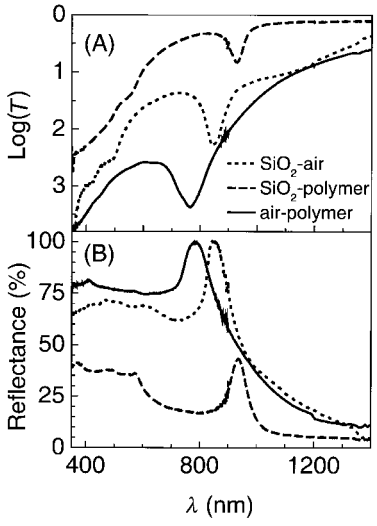

Fig. 4. Transmission (A) and angle integrated reflectance (B) from a 390 nm sphere opal: before infiltration (dotted line), after infiltration (dashed line), and after inversion (solid line).

(74 % silica, 26 % polymer) and the solid line to the inverse opal (74 % air, 26 % polymer). It can readily be seen that both the attenuation and the diffuse reflection increase as the dielectric contrast does and the filling fraction of the higher refractive index component decreases. This accounts for the reduction in attenuation and reflectance attained when the bare opal is filled with polymer since the dielectric constants of polymer and silica are closer than those of silica and air. On this line of reasoning the increase in scattering observed on inversion is due to the enhanced contrast between polymer and air. The propagation along different crystalline directions were also studied. Transmission experiments at different incidence angles with respect to the (111) planes were performed.

The optical properties, as far as positions and widths of the pseudogaps are concerned, can be accounted for by photonic band calculations. Our calculations have been performed using a plane wave basis in an iterative implementation.[15] Theory and experiments are summarized in Figure 5 for a sample of 390 nm sphere diameter. In the left panel of Figure 5 experimental reflectance spectra obtained at normal

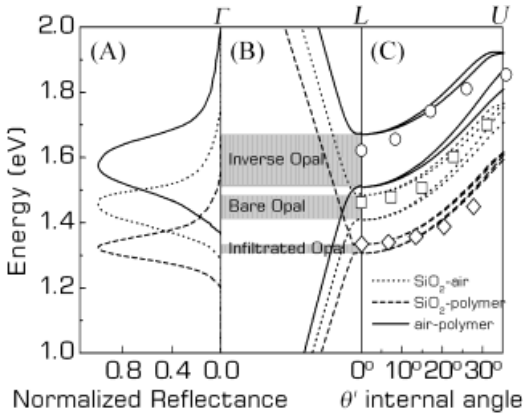

Fig. 5. A) Experimental reflectance spectra: dotted, dashed, and solid lines correspond to the bare, composite, and inverse opals, respectively. The diffuse background has been subtracted and the intensity normalized to its maximum. B) Calculated band diagrams along *Γ*–*L* direction for the bare, the infiltrated and the inverse opal. Different line types have the same meaning as in (A). C) Band diagram for *L*–*U* path together with the experimental pseudogap center represented as symbols (see text).

incidence with respect to the (111) planes are shown for the three systems (dotted line for the bare opal, dashed lines for the polymer–silica composite, and solid lines for the polymer inverse opal). The center panel shows, with the same convention, those bands that lie in the corresponding direction, *Γ*–*L*. The agreement theory–experiment is fairly good, not only regarding positions, but also regarding widths. Finally, in the right hand side panel, we have plotted the energy of the reflection peak on top of the bands along the *L*–*U* path as a function of the internal angle measured with respect to the *L* direction. Here squares, diamonds, and circles stand for the reflectance peak position as the sample is tilted off the (111) direction for bare opal, composite and inverse structure respectively. In view of the fact that the photonic band structure is rather isotropic around the *L* point, we have chosen the *L*–*U* direction as representative of the behavior of energy bands, the points *W* and *K* being very much the same as *U*. Inspection of the energy diagram around the *L* point reveals that states near those points are very similar irrespective of their particular wavevector.

Since the underlying structure is unchanged on filling or inversion, the lattice parameter remains the same and, as a consequence, the energy position of the *L* pseudogap is, fundamentally, determined by the average dielectric constant. This explains the relative positions in Figure 5. For the bare opal

  0935-9648/01/0603-0395 $ 17.50+.50/0

ADVANCED MATERIALS

the average dielectric constant is $\langle\varepsilon\rangle$ = 1.94, and increases to $\langle\varepsilon\rangle$ = 2.22 in the infiltrated one (reducing the contrast at the same time). After inversion the mean dielectric constant decreases to $\langle\varepsilon\rangle$ = 1.41 and, accordingly, the *L* pseudogap energy shifts upwards (see Fig. 5).

The peak width is a function of both the dielectric contrast and the filling factor of the structure. Bare opals present a contrast $\varepsilon_{SiO_2}/\varepsilon_{air}$ = 2.1 that shifts to $\varepsilon_{polymer}/\varepsilon_{SiO_2}$ = 1.24 when infiltration takes place. So, the pseudogap width is largely decreased, as is observed in both the experiment and band structure calculation. When inversion occurs, the dielectric contrast is increased up to $\varepsilon_{polymer}/\varepsilon_{air}$ = 2.6. It has to be noticed that, although bare and inverse opal have similar values of the refractive index contrast, inverse opals show a much broader pseudogap than the direct opal structure which reflects the fact that inverse structures are more powerful scatterers (see Fig. 5A).

When the sample is tilted with respect to normal incidence, the ***k*** vector ceases to be collinear with *Γ*–*L*. For a given direction (tilt angle), at some point of the energy scan, ***k*** crosses the Bragg plane and a reflection is obtained. Since *L* is the closest (to *Γ*) point of the Bragg plane, tilting increases both the wavevector length and the energy for which reflection occurs. This pseudogap energy position, can be followed along the *L*–*U* (or *L*–*K* or *L*–*W*) line in the Brillouin zone. In Figure 5C experimental data are superimposed on the band structure diagram by using Snell's law with an average refractive index for calculating the internal angle (with respect to the *Γ*–*L* direction). The theory gives a good account of the behavior of the pseudogap position.

In summary, we have obtained and optically analyzed polymer inverse opals with a long-range order. Their photonic crystal behavior has been studied both experimentally and theoretically, and a good agreement between band-structure calculations and experiments was found. From a fundamental point of view, they can be regarded as model systems, where studying the effect of topology and dielectric contrast is possible. Regarding their potential applications, they can be used to modify the emission properties of luminescent species, such as dyes, that can easily be incorporated into the polymer. Polymer inverse opals offer, in turn, the interesting possibility of being used as matrices to obtain new spherical colloidal particles, whose shape cannot be controlled otherwise, from different materials.

Experimental

The polymer used for infiltration was obtained by the polymerization of 15 cm^3 of an epoxy resin (Bisphenol A-epichlorhydrine, Struers) in the presence of 2 cm^3 of catalyzer (Triethylentetramin, Struers). In this way a viscous fluid is obtained in which the opal is immersed. The liquid soaks the opal and when the diffusion is completed the opal turns transparent as a consequence of the partial-index matching between silica and polymer. In about 12 h polymerization completes and the shrinkage between the liquid and the solid is less than 5 %. This allows a good filling and a very good connection of the infiltrated material. The polymer refractive index was measured by the prism minimum deviation angle and resulted to be n = 1.609 ± 0.005.

Once the infiltrated polymer has solidified, the block is cut and polished until the original outer facet of the opal is brought to the surface of the block. The same is done on the rear surface to finally obtain a sample about 200 μm thick. The polishing is carried out with alumina powder down to 0.05 μm roughness.

Received: October 5, 2000

[1] J. D. Joannopoulos, R. D. Meade, J. N. Winn, *Photonic Crystals*, Princeton University Press, Princeton, NJ **1995**.
[2] J. D. Joannopoulos, P. R. Villeneuve, S. Fan, *Nature* **1997**, *386*, 143.
[3] R. Mayoral, J. Requena, S. J. Moya, C. López, A. Cintas, H. Míguez, F. Meseguer, L. Vázquez, M. Holgado, A. Blanco, *Adv. Mater.* **1997**, *9*, 257.
[4] Y. A. Vlasov, V. N. Astratov, O. Z. Karimov, A. A. Kaplyanskii, V. N. Bogomolov, A. V. Prokofiev, *Phys. Rev. B* **1997**, *55*, 13 357.
[5] H. Míguez, C. López, F. Meseguer, A. Blanco, L. Vázquez, R. Mayoral, M. Ocaña, A. Mifsud, V. Fornés, *Appl. Phys. Lett.* **1997**, *71*, 1148.
[6] S. H. Park, Y. Xia, *Adv. Mater.* **1998**, *10*, 1045.
[7] S. A. Johnson, P. J. Oliver, T. E. Mallouk, *Science* **1999**, *283*, 963.
[8] K. Yoshino, S. B. Lee, S. Tatsuhara, Y. Kawagishi, M. Ozaki, A. A. Zakhidov, *Jpn. J. Appl. Phys. 2* **1999**, *38*, L786.
[9] K. Yoshino, S. B. Lee, S. Tatsuhara, Y. Kawagishi, M. Ozaki, A. A. Zakhidov, *Appl. Phys. Lett.* **1999**, *73*, 3506.
[10] J. F. Bertone, P. Jiang, K. S. Hwang, D. M. Mittleman, V. Colvin, *Phys. Rev. Lett.* **1999**, *83*, 300.
[11] C. López, H. Míguez, F. Meseguer, R. Mayoral, L. Vázquez, M. Ocaña, *Superlattices Microstruct.* **1997**, *22*, 399. H. Míguez, F. Meseguer C. López, A. Mifsud, J. S. Moya, L. Vázquez, *Langmuir* **1997**, *13*, 6009.
[12] G. H. Bogush, M. A. Tracy, C. F. Zukoski. *J. Non-Cryst. Solids* **1988**, *104*, 95.
[13] H. Míguez, F. Meseguer, C. López, A. Blanco, J. S. Moya, J. Requena, A. Mifsud, V. Fornés, *Adv. Mater.* **1998**, *10*, 480.
[14] E. Matijevic, *Langmuir* **1994**, *10*, 8.
[15] R. Meade, A. M. Rappe, K. D. Rommer, J. D. Joannopoulos, *Phys. Rev. B* **1993**, *48*, 8434. Erratum by S. G. Johnson, *Phys. Rev. B* **1997**, *55*, 15 942.

Structured Metallic Films for Optical and Spectroscopic Applications via Colloidal Crystal Templating**

By *Peter M. Tessier*, *Orlin D. Velev*,* *Anand T. Kalambur*, *Abraham M. Lenhoff*, *John F. Rabolt*, and *Eric W. Kaler*

Porous metallic films are promising structures for applications in photonic materials, sensors, catalysts, and energy-harvesting coatings. Here we describe how e-beam and other complex microfabrication techniques for forming such films can be replaced by a simple wet-chemistry templating method. The pores are templated by two-dimensional (2D) crystals of latex microspheres embedded into a structure assembled from gold nanoparticles. The porous metallic films formed by this method have interesting optical properties and are excellent substrates for surface-enhanced Raman spectroscopy (SERS).

[*] Prof. O. D. Velev, P. M. Tessier, Prof. A. M. Lenhoff, Prof. E. W. Kaler
Center for Molecular and Engineering Thermodynamics
Department of Chemical Engineering
University of Delaware
Newark, DE 19716 (USA)
E-mail: Velev@che.udel.edu
A. T. Kalambur, Prof. J. F. Rabolt
Department of Materials Science and Engineering
University of Delaware
Newark, DE 19716 (USA)

[**] We thank Yonghui Yuan and Rajesh Pazhianur for their help with AFM imaging and George Watson for helpful discussions.

  0935-9648/01/0603-0396 $ 17.50+.50/0